Desalination and Water Treatment
www.deswater.com
doi: 10.5004/dwt.2018.22609

127 (2018) 325–333
September

One-step surface-functionalization of polydopamine-modified multiwalled carbon nanotubes for the selective removal of organic dyes from aqueous solutions

Fangli Liao*, Kejun Feng, Luigi Agostini, Xianfeng Li

School of Chemistry and Materials Engineering, Huizhou University, Huizhou 516007, China, emails: 1628640576@qq.com (F. Liao), 466399081@qq.com (K. Feng), luigiago@hotmail.com (L. Agostini), 252756005@qq.com (X. Li)

Received 7 November 2017; Accepted 6 June 2018

ABSTRACT

Multiwalled carbon nanotubes (MWCNTs) modified by polydopamine (PDA) (MWCNTs/PDA) were synthesized via oxidation polymerization of dopamine. Scanning electron microscopy, Fourier transform infrared spectroscopy, and thermogravimetric analyses were used to characterize the obtained materials. To study the effect of the mass fraction of PDA on the adsorption capacity, a series of MWCNTs/PDA composites with different mass ratios between MWCNTs and PDA, were prepared, and their adsorption selectivity toward six different dyes was investigated. The results indicated that the MWCNTs/PDA composite with a 1:1 mass ratio between MWCNTs and PDA exhibits a higher adsorption capacity toward phenazine and phenothiazine dyes, which both contain the C=C–C=N 1,4-conjugate quinone structure and acid fuchsin, with a N atom in a C=C–C=N 1,4-conjugate structure connecting H atoms. The adsorption process could be well described by the pseudo-second-order kinetic model and by the Langmuir isotherm, respectively. Furthermore, thermodynamic parameters revealed that the adsorption was an endothermic and spontaneous process.

Keywords: Adsorption; Multiwalled carbon nanotubes; Polydopamine; Organic dyes; Neutral red

1. Introduction

Over the past few decades, discharge of industrial effluents containing organic dyes has brought about serious environmental pollution which threatens human health [1–3]. Therefore, owing to their ubiquitous use in many industries, removal of organic dyes from polluted water has been an important research subject [4]. Several biological treatments, physicochemical strategies, and chemical methods have been extensively investigated to alleviate the effluent pollution, such as photocatalysis [5,6], chemical precipitation [7,8], electrochemical degradation [9,10], ozonation [11,12], advanced oxidation processes [13,14], membrane filtration [15,16], and adsorption [17–19]. However, most techniques have their inherent limitations, including the excessive usage of chemicals, expensive plant requirements, and high operational costs. Among these methods, adsorption may be regarded as a superior technology, due to its high efficiency, easier operation, and low operational cost.

To date, many types of adsorbents, possessing selective adsorption, and capable of eliminating dyes from wastewater, have been studied, such as inorganic or organic modified carbon-based nanoparticles [20–22], wood waste [23], inorganic materials [24], metal-organic frameworks [25], supramolecular hydrogels [26], and polymers [27–29]. Especially, multiwalled carbon nanotubes (MWCNTs), as carbon-based nanomaterials, have been widely applied as promising adsorbents due to their unique quasi-one dimensional hollow structure, high specific surface areas, light weight, and good chemical stability [30–32]. However, their selectivity is usually realized by introducing functional groups onto their surfaces [33,34]. Polymers usually exhibit different kind of functional groups, such as

* Corresponding author.

hydroxyl, carboxyl, or amidogen, which could improve adsorption capacity via noncovalent host–guest interactions (electrostatic interaction, Van der Waals forces, π–π stacking interaction, and hydrophobic interaction) between the adsorbent and the dye molecules [34–36]. Polydopamine (PDA), which can be synthesized through the spontaneous polymerization of dopamine in aerobic atmosphere under alkaline conditions, contains functional groups, including catechol, amine, and imine, beneficial to the adsorption process [37–40]. In addition, dopamine, a mussel-inspired protein, can form surface-adherent PDA films onto various inorganic and organic materials [41–43].

Based on these unique features, the objective of this work is to synthesize PDA-coated MWCNT (MWCNT/PDA) composites and investigate their adsorption behavior for dyes. To study the effect of PDA's mass fraction on the adsorption capacity, a series of MWCNTs/PDA composites, with different mass fraction of PDA, were easily prepared through a spontaneous polymerization method. The results show that the adsorption capacity of MWCNTs/PDA is highest when the mass ratio between MWCNTs and PDA is 1:1. Further, we selected the following six dyes: neutral red (NR), acid fuchsin (AF), azure A (AZA), methylene blue (MB), rhodamine B (RHB), and alizarin red S (ARS), to study the selective adsorption ability of MWCNTs/PDA composites. Finally, the influence (influential) of factors, such as contact time, solution pH, and temperature, were tested. The adsorption isotherms, kinetics, and thermodynamics were also investigated.

2. Experimental

2.1. Materials

All chemicals were of analytical grade and used as received without further purification. Deionized water used in all experiments was purified using the Milli-Q water purification system. MWCNTs were purchased from Shenzhen Nanotech Port Co., Ltd., Shenzhen, China. Dopamine (DA) hydrochloride and tris(hydroxymethyl)aminomethane (Tris) were obtained from Tianjin Hengxing Chemical Reagent Co., Ltd., Tianjin, China. NR, AF, AZA, MB, RHB, ARS, hydrochloric acid, and sodium hydroxide were supplied by Sinopharm Chemical Reagent Co., Ltd., Shanghai, China.

2.2. Instrumentation

The absorbance of dyes was detected by a 752 UV-Vis spectrophotometer. A Nicolet 6700 Fourier transform infrared (FTIR) spectrometer (Thermo Fisher Scientific, USA) was used to confirm whether the DA was polymerized on the surface of MWCNTs successfully or not. Scanning electron microscopy (SEM) images of the absorbents were performed using a MIRA3 scanning electron microscope (TESCAN, Czech). Thermogravimetric analyses (TGA) were conducted on a SDT Q600 thermal analyzer (TA Instruments, USA) to further estimate the relative composition of nanoparticles.

2.3. Synthesis of MWCNTs/PDA

100 mg MWCNTs were dispersed in 100 mL of Tris–HCl buffer solution (10 mM, pH = 8.5) and ultrasonically treated for 10 min to obtain homogeneous dispersion. Then 50, 100, 150, or 200 mg of DA were dissolved in the mixed solution, respectively. After mechanical agitation for 24 h at 35°C under anaerobic atmosphere, the deep brown solution was separated by a 0.45 μm polytetrafluoroethylene membrane and the filtrate was washed with deionized water until removal of the unpolymerized dopamine monomer, then dried under vacuum at 40°C for 24 h. The obtained MWCNTs/PDA composites were marked, respectively, as MWCNTs/PDA (2:1), MWCNTs/PDA (1:1), MWCNTs/PDA (2:3), and MWCNTs/PDA (1:2), according to their mass fraction of PDA. Fig. 1 shows the process for the modification of MWCNTs.

2.4. Dyes adsorption experiments

For the contrast experiments, six typical dyes, namely NR, AF, AZA, MB, RHB, and ARS were chosen as absorbates to investigate the adsorption capacity of different absorbents: raw MWCNTs, MWCNTs/PDA (2:1), MWCNTs/PDA (1:1), MWCNTs/PDA (2:3), and MWCNTs/PDA (1:2). The chemical structures of the dyes are shown in Fig. 2. The equilibrium adsorption capacity (q_e) was obtained through the following typical adsorption experiment: 5.0 mg of absorbent and 20 mL of dye solution, of known initial concentration, were mixed together in 50 mL conical flask, then the mixture was stirred continuously at 25°C until equilibrium was reached. The absorbance of the residual dye in solution was measured by using a 752 UV-Vis spectrophotometer operating at a wavelength corresponding to the maximum absorption wavelength of the dye. The equilibrium concentration of each dye was calculated according to the standard calibration curve. The q_e can be determined by the following formula [44]:

$$q_e = \frac{(C_o - C_e)V}{m} \tag{1}$$

where q_e (mg/g) is the equilibrium adsorption capacity of absorbent. C_0 and C_e (mg/L) are the initial and equilibrium concentrations of dye. V (L) is the volume of the aqueous solution and m (g) is the mass of adsorbent.

Moreover, NR and MWCNTs/PDA (1:1) were selected as representative absorbate and absorbent to run a series of experiments to study the effect of crucial parameters, such as contact time (0–180 min), pH (2.0–7.0), temperature (298–318 K), and initial dye concentration (5.0–30.0 mg/L), on the final equilibrium concentration q_e.

For kinetic studies, 20 mL of dye solution (the initial concentration of which was 20.0 mg/L) and 5.0 mg of absorbent

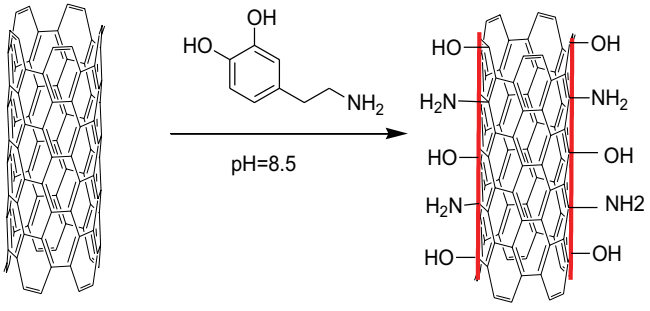

Fig. 1. Schematic representation of the modification of MWCNTs.

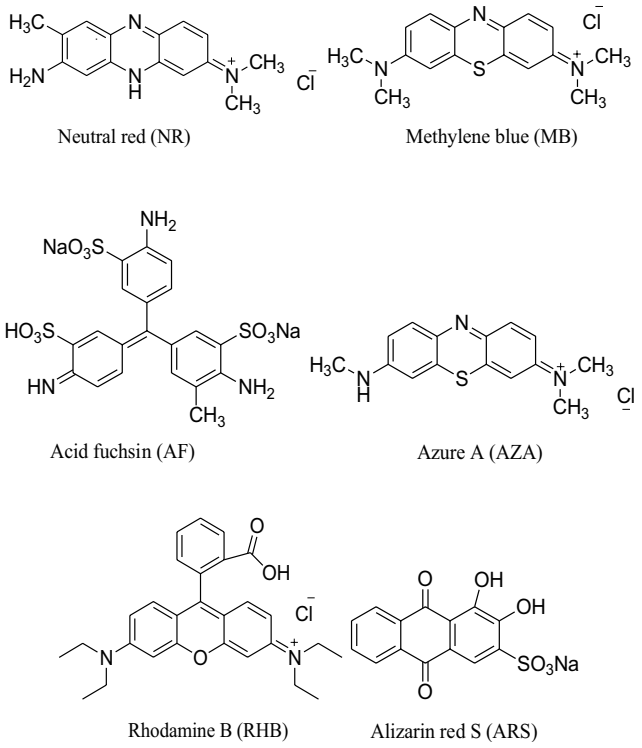

Fig. 2. The chemical structure of dyes tested in this work.

were put together in a 50 mL conical flask. Thereafter, nine independent flasks were shaken in a constant temperature (25°C) shaking water bath for different contact time (0–180 min). At various time intervals, the sediment was removed by filtering the mixture with MCE (mixed cellulose acetate and cellulose nitrate ester) membrane discs (pore size 0.45 μm). The concentration of dye in the supernatant was analyzed by UV-Vis spectrophotometer.

For adsorption isotherm, 20 mL of dye solution (the initial concentration of which was 5.0–30.0 mg/L) and 5.0 mg of absorbent were mixed together in a 50 mL conical flask and shaken for 30 min at 298, 308, and 318 K, respectively. Then, the equilibrium concentration of dye was measured.

The effect of solution pH was investigated by mixing 20 mL of dye solution (the initial concentration of which was 20.0 mg/L) and 5.0 mg absorbent in a 50 mL conical flask and shaking for 30 min at different pH levels (2.0–7.0). The pH of dye solution was adjusted using HCl (0.10 mol/L) and NaOH (0.10 mol/L) solutions. Then, the final dye concentration was measured.

3. Results and discussion

3.1. Characterization of MWCNTs/PDA

Figs. 3(a)–(e) are the SEM images of raw MWCNTs, MWCNTs/PDA (2:1), MWCNTs/PDA (1:1), MWCNTs/PDA (2:3), and MWCNTs/PDA (1:2), respectively, which show the morphology and microstructure of absorbents. It can be seen that, compared with raw MWCNTs (Fig. 3(a)), the surface of MWCNTs/PDA (Figs. 3(b)–(e)) became significantly rougher. In addition, with the increase of the dopamine content, the tendency of accumulation and aggregation became more significant, the distribution of PDA in MWCNTs/PDA (1:1) was the most uniform among all the obtained composites (Fig. 3(c)), and such uniform distribution improved its adsorption capacity. Table 1 shows the elemental analysis of raw MWCNTs and MWCNTs/PDA, demonstrating that PDA had been successfully polymerized on the surface of MWCNTs. Moreover, by decreasing the mass ratio between

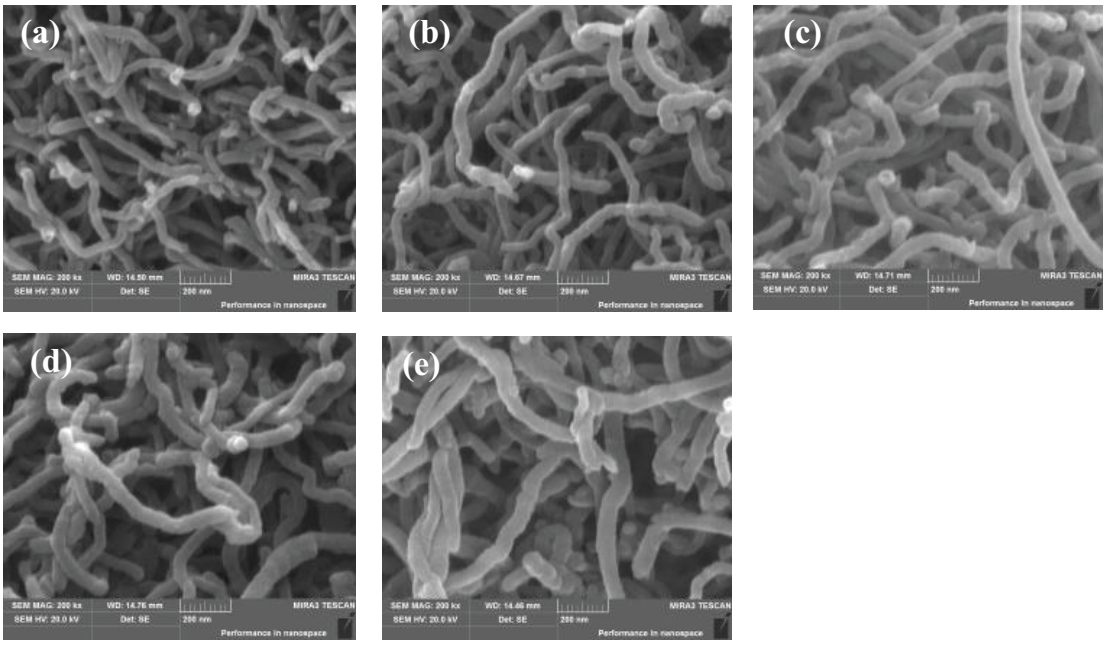

Fig. 3. SEM images of (a) MWCNTs, (b) MWCNTs/PDA (2:1), (c) MWCNTs/PDA (1:1), (d) MWCNTs/PDA (2:3), and (e) MWCNTs/PDA (1:2).

Table 1
The contents of elements in materials

Materials	N (%)	C (%)	O (%)
r-MWCNTs	2.97	95.65	1.38
MWCNTs/PDA (2:1)	3.67	87.21	9.12
MWCNTs/PDA (1:1)	5.98	83.00	11.11
MWCNTs/PDA (2:3)	5.33	82.20	12.46
MWCNTs/PDA (1:2)	6.67	76.47	16.86

MWCNTs and PDA from 2:1 to 1:2, the elemental content of N increased from 3.67% to 5.89%. However, by comparing MWCNTs/PDA (1:1) and MWCNTs/PDA (1:2), we found that despite the latter's amount of dopamine doubled, there was only a 1% increase in the elemental content of N. Therefore, we drew the conclusion that the utilization of dopamine in MWCNTs/PDA (1:1) was the highest.

FTIR spectra of raw MWCNTs and MWCNTs/PDA composites are shown in Fig. 4(a), in the range of 500–4,000 cm^{-1}, to exhibit the absorption peaks of the composites' functional groups The characteristic wide peak at 3,445 cm^{-1} is due to the stretching vibration of υ(OH). For the MWCNTs/PDA composites, the characteristic peak at 3,552 cm^{-1} is assigned to the stretching vibration of υ(NH). Finally, the adsorption at 700–750 cm^{-1} can be ascribed to the bending vibration (out-plane bending vibration) of N–H band. Evidently, these peaks indicate the successful coating of PDA on MWCNTs.

TGA was performed on a thermal analyzer in the temperature region of 25°C–800°C (as shown in Fig. 4(b)) to further estimate the amount of polymers grafted onto the MWCNTs and the thermal stability of materials. The weight loss of water in external surface and internal pores or cavities was below 200°C. The PDA decomposed entirely at about 650°C. It can be seen from the TGA curves that the contents of PDA coated on the MWCNTs/PDA (2:1), MWCNTs/PDA (1:1), MWCNTs/PDA (2:3), and MWCNTs/PDA (1:2) were 17.90%, 26.58%, 26.59%, and 26.68%, respectively. The above result further proves that the preparation of composites was successful and the yield of PDA in MWCNTs/PDA (1:1) was the highest.

3.2. Contrast adsorption experiments

The adsorption behavior of synthesized MWCNTs/PDA toward six different dyes was studied and the results are exhibited in Figs. 5(a)–(f). According to the figures, the adsorption capacities of MWCNTs/PDA composites toward NR, AF, AZA, and MB are superior to that of raw MWCNTs. And the adsorption capacities increased by increasing the mass ratio of PDA from 2:1 to 1:1, then decreased from 1:1 to 1:2, that is, which means that, MWCNTs/PDA (1:1) exhibited the highest adsorption capacity. The different adsorption capacity of the MWCNTs/PDA composites with different amount of dopamine is due to the synergistic effect of MWCNTs and dopamine. The SEM images of synthesized MWCNTs/PDA composites shown in Figs. 3(a)–(e) may explain why the adsorption capacity of MWCNTs/PDA (1:1) was the highest. First of all, the PDA coating is necessary in

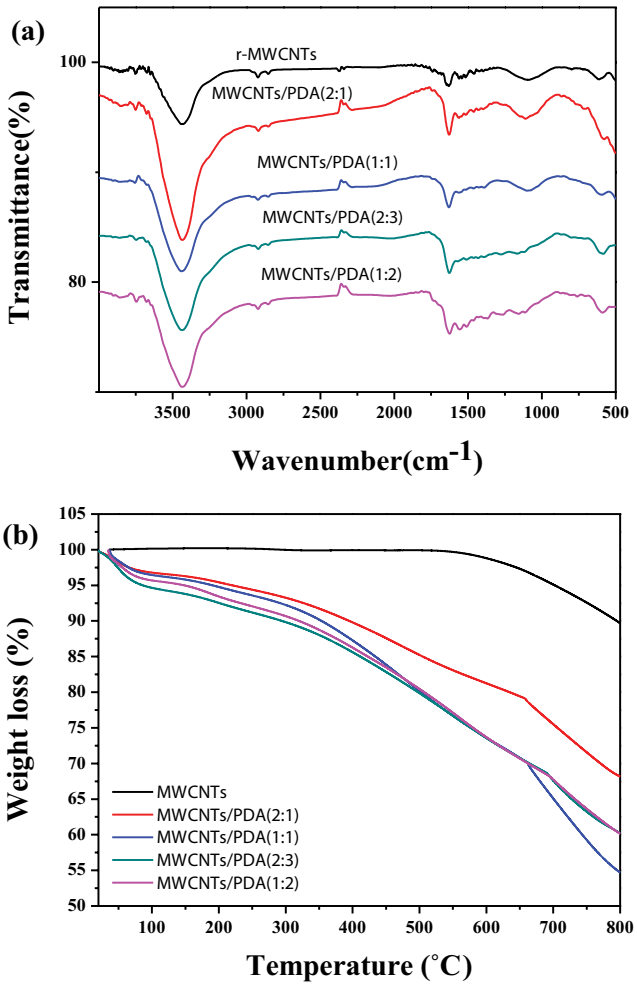

Fig. 4. (a) The FTIR spectra of MWCNTs, MWCNTs/PDA (2:1), MWCNTs/PDA (1:1), MWCNTs/PDA (2:3), and MWCNTs/PDA (1:2). (b) The TGA curves of MWCNTs, MWCNTs/PDA (2:1), MWCNTs/PDA (1:1), MWCNTs/PDA (2:3), and MWCNTs/PDA (1:2).

order to achieve high adsorption capacity, and the distribution of PDA on the surface of MWCNTs/PDA (1:1) (Fig. 3(c)) is the most uniform, which translates in more active sites for the adsorption of dyes. Further, roughened surface, with large specific surface area, is conductive to an increase of the adsorption capacity. However, excessive PDA coating on MWCNTs would lead to a reduction in adsorption capacity, owing to only increasing the weight of material and not in the creation of more active sites for adsorption.

On the contrary, for the other two dyes: RHB and ARS, the adsorption capacities of as-prepared materials were lower than that of raw MWCNTs. A closer look at the chemical structures of these six dyes may explain this phenomenon. NR as phenazine dye, MB and AZA as phenothiazine dye, all contain the C=C–C=N 1,4-conjugate quinone structure, which is beneficial to the improvement of the adsorption capacity via electrostatic attraction, π–π stacking interaction, Van der Waals forces, and 1,4-Michael addition reaction between adsorbent and dyes. However, in the chemical structure of RHB, although it contains the

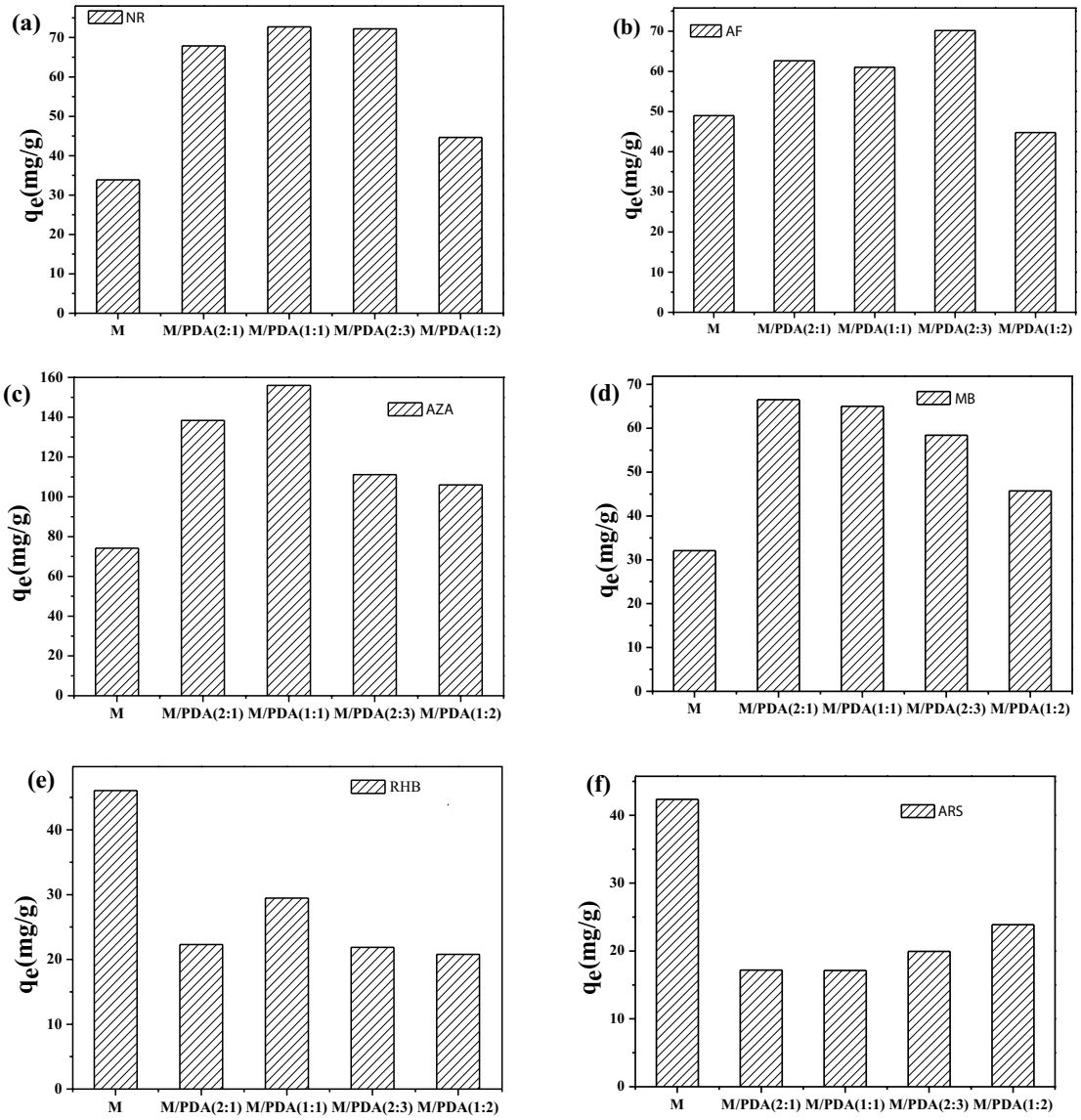

Fig. 5. (a–f)The adsorption capacity of synthesized materials toward NR, AF, AZA, MB, RHB, and ARS, respectively (M stands for MWCNTs).

C=C–C=N 1,4-conjugate structure, the nitrogen atom is connected with two ethyl chains rather than H atoms as in AF. Therefore, the steric hindrance created by the carbon chains leads to the decrease of the adsorption capacity of MWCNTs/PDA. In the chemical structure of ARS, the group of catechol tends to form intramolecular hydrogen bonds, rather than intermolecular hydrogen bonds between absorbent's molecules, via host–guest interactions, as a result, the adsorption capacity of MWCNTs/PDA is lower than that of raw MWCNTs. Thus, for the further experiments, MWCNTs/PDA (1:1) was chosen as absorbent and NR was used as a representative absorbate.

3.3. Effect of pH

To further analyze the adsorption process, the pH of the dye solution, which could affect aqueous chemistry and surface binding sites of the adsorbents, was investigated. Fig. 6(a) shows the results. As it can be seen, the adsorption capacity of MWCNTs/PDA (1:1) was directly proportional to the pH of the solution in the range from 2.0 to 7.0, that is, when the pH value of the NR solution was 7 the adsorption capacity of MWCNTs/PDA (1:1) was optimal. This trend can be explained by considering the structure of the absorbent. The electron cloud density of phenolic hydroxyl group on the absorbent increased with the increase of the pH value, which contributes to the formation of host–guest interaction with NR. Therefore, the adsorption capacity of the absorbent increased.

3.4. Effect of contact time

The influence of contact time on the adsorption process was also investigated in order to determine the equilibrium

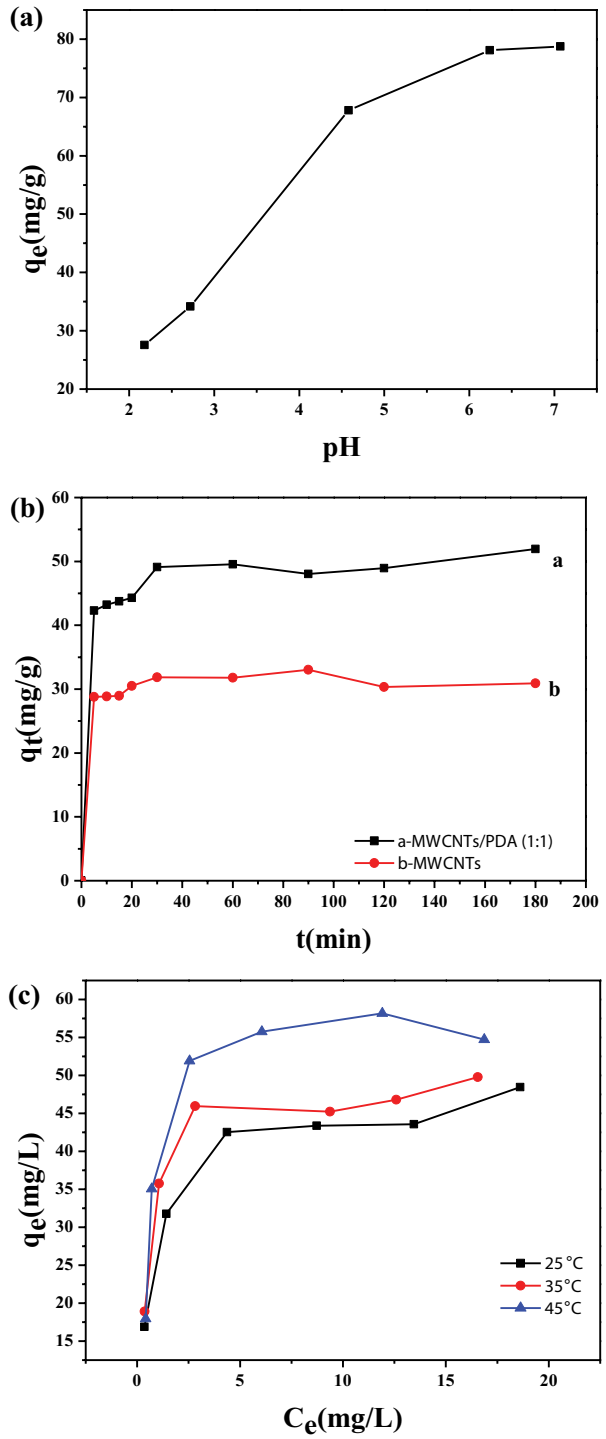

Fig. 6. (a) Effect of pH on the adsorption capacity of MWCNTs/PDA (1:1) toward NR at 25°C,(b) effect of time on the adsorption of NR onto MWCNTs and MWCNTs/PDA (1:1), and (c) effect of temperature on the adsorption of NR onto MWCNTs/PDA (1:1).

time. The adsorption capacity of MWCNTs/PDA and MWCNTs toward NR at various time is shown in Fig. 6(b). It is obvious that the adsorption capacity increased drastically during the first 5 min and reached equilibrium at 30 min. Fig. 6(b) also shows that the maximum adsorption quantity of MWCNTs and MWCNTs/PDA (1:1) was 30.92 and 51.95 mg/g, respectively. The adsorption capacity of modified material was almost double than that of raw MWCNTs.

3.5. Effect of temperature

Temperature is also an important parameter influencing the adsorption process. As shown in Fig. 6(c), the adsorption capacity increased while increasing the experimental temperature from 298 to 318 K, which indicated that higher temperatures were more beneficial to the adsorption and that the adsorption of NR onto MWCNTs/PDA (1:1) was an endothermic process.

3.6. Kinetic studies

Kinetic studies of MWCNTs/PDA (1:1) toward NR, which could provide valuable insight into the adsorption process, were also conducted. Two kinetic models, the pseudo-first-order and the pseudo-second-order were used in this study to investigate the mechanism of adsorption [45]. These models are both expressed in linear form.

The pseudo-first-order kinetic model is expressed as:

$$\log\left(q_e - q_t\right) = \log q_e - \frac{k_1 t}{2.303} \tag{2}$$

where q_e (mg/g) and q_t (mg/g) are the adsorption capacity at equilibrium and any time t (min), respectively. k_1 (min^{-1}) is the pseudo-first-order rate constant.

The pseudo-second-order model is represented as the following form:

$$\frac{t}{q_t} = \frac{1}{k_2 q_e^2} + \frac{t}{q_e} \tag{3}$$

where k_2 (g/mg/min) is the rate constant of the pseudo-second-order model.

The parameters of the two kinetic equations are summarized in Table 2 and the fitting lines of the pseudo-second-order model are shown in Fig. 7(a). As shown in Table 2, the correlation coefficient (R^2) of the pseudo-second-order was higher than 0.99 and the calculated adsorption capacity (q_e = 51.57 mg/g) for the pseudo-second-order model was very close to the one obtained experimentally (q_t = 51.95 mg/g). Therefore the adsorption of NR can be explained by the pseudo-second-order model.

3.7. Adsorption isotherm studies

A series of experiments were carried out to study the adsorption behavior of NR onto MWCNTs/PDA (1:1).

Table 2
Kinetic parameters for the adsorption of NR onto MWCNTs/PDA (1:1)

Pseudo-first-order model			Pseudo-second-order model		
q_e (mg/g)	k_1 (min^{-1})	R^2	q_e (mg/g)	k_2 (g/mg/min)	R^2
12.32	0.02374	0.7181	51.57	0.007063	0.9980

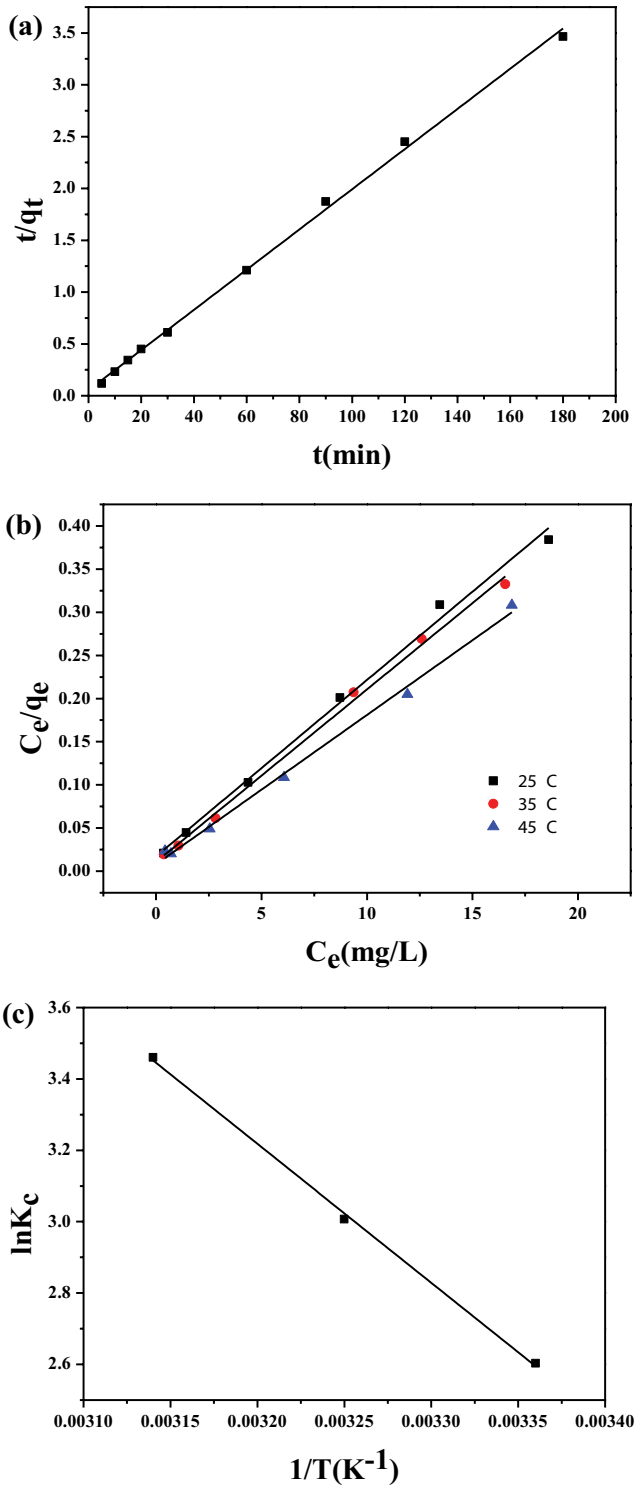

Fig. 7. (a) Pseudo-second-order model for the adsorption of NR onto MWCNTs/PDA (1:1), (b) the curve-fitting lines of Langmuir isotherm, and (c) plot of ln K_c versus 1/T for the adsorption of NR.

The linear form of Langmuir and Freundlich isotherms was used to analyze the adsorption mechanism [46]. The Langmuir isotherm, which is suitable to model monolayer adsorption with homogeneous sites, is given by the following expression:

$$\frac{C_e}{q_e} = \frac{1}{b \times q_m} + \frac{C_e}{q_m} \tag{4}$$

where q_e (mg/g) is the adsorption capacity at equilibrium. C_e (mg/L) is the equilibrium concentration of the dye in solution. q_m (mg/g) is the calculated maximum adsorption capacity and b (L/mg) is the constant of Langmuir isotherm.

The Freundlich isotherm instead, which can be used to model multilayer adsorption, is given by the following expression:

$$\ln q_e = \ln k_f + \frac{1}{n} \ln C_e \tag{5}$$

where k_f (L/mg) and n are the Freundlich constants.

The fitting parameters of the two isotherms are shown in Table 3. Fig. 7(b) shows the curve-fitting lines for the Langmuir isotherm. According to the obtained data, Langmuir isotherm with higher R^2 values was the optimal candidate to describe the monolayer adsorption of NR on MWCNTs/PDA (1:1). Furthermore, the values of q_m obtained from Langmuir isotherm were fitted well with the experimental adsorption capacity, which shows that the adsorption sites of MWCNTs/PDA (1:1) were homogeneous.

3.8. Thermodynamics studies

Different thermodynamic parameters, standard free energy ($\Delta G°$), enthalpy ($\Delta H°$), and entropy ($\Delta S°$), summarized in Table 4, were calculated via the following equations [47]:

$$\Delta G° = -RT \ln K_c \tag{6}$$

$$-RT \ln K_c = \Delta H° - T\Delta S° \tag{7}$$

Table 3
The isotherm constants of Langmuir and Freundlich model

Model	Parameter	Parameter value		
		25°C	35°C	45°C
Langmuir isotherm	q_m (mg/g)	48.924	50.025	57.770
	B (L/mg)	1.190	1.861	2.172
	R^2	0.9940	0.9965	0.9953
Freundlich isotherm	1/n	4.405	4.702	3.783
	k (L/mg)	25.208	29.360	31.376
	R^2	0.8698	0.7211	0.6888

Table 4
Thermodynamic parameters for the adsorption of NR onto MWCNTs/PDA (1:1)

$\Delta H°$ (kJ/mol)	$\Delta S°$ (J/K mol)	T (K)	$\Delta G°$ (kJ/mol)	R^2
32.392	130.409	298	–6.470	0.9978
		308	–7.774	
		318	–9.078	

$$\ln K_c = \frac{\Delta S^{\Theta}}{R} - \frac{\Delta H^{\Theta}}{RT} \quad (8)$$

where K_c is the equilibrium distribution coefficient for the adsorption process, which is calculated through the following equation:

$$K_c = \frac{C_0 - C_e}{C_e} \quad (9)$$

R (8.314 J/(mol K)) is the gas constant and T (K) is the absolute temperature. $\Delta H°$ and $\Delta S°$ can be determined by the slope and intercept of the plot of ln K_c versus $1/T$ as shown in Fig. 7(c). As it can be seen from Table 4, the process of adsorption is an endothermic process owing to the positive value of $\Delta H°$ and therefore lower temperature would facilitate the removal of NR. The negative value of $\Delta G°$ suggested that the adsorption of NR is spontaneous in nature.

4. Conclusion

In summary, PDA-coated MWCNTs were synthesized by oxidation polymerization of DA under basic condition and fully characterized. To study the effect of the mass fraction of PDA on the adsorption capacity, a series of MWCNTs/PDA composites, with different mass ratio between MWCNTs and PDA, were prepared. Subsequently, systematical experiments were conducted to investigate their adsorption selectivity toward six different dyes. The results showed that MWCNTs/PDA (1:1) exhibited an excellent adsorption capacity toward phenazine and phenothiazine dyes, that contains C=C–C=N 1,4-conjugate quinone structure, and toward AF with N atom in a C=C–C=N 1,4-conjugate structure connecting H atoms. The adsorption capacity of MWCNTs/PDA (1:1) toward NR was 58.17 mg/g at an initial NR concentration of 25.0 mg/L. Meanwhile, the adsorption study showed that the pseudo-second-order model and Langmuir isotherm were more suitable to explain the adsorption process. Furthermore, thermodynamic parameters revealed that the adsorption was an endothermic and spontaneous process. In conclusion, MWCNTs/PDA (1:1) proved to be an extremely powerful composite material for removing dyes from aqueous solutions.

References

[1] E. Kordouli, K. Bourikas, A. Lycourghiotis, C. Kordulis, The mechanism of azo-dyes adsorption on the titanium dioxide surface and their photocatalytic degradation over samples with various anatase/rutile ratios, Catal. Today, 252 (2015) 128–135.

[2] H. Sayğılı, F. Güzel, Y. Önal, Conversion of grape industrial processing waste to activated carbon sorbent and its performance in cationic and anionic dyes adsorption, J. Cleaner Prod., 93 (2015) 84–93.

[3] M.X. Wang, Q.L. Zhang, S.J. Yao, A novel biosorbent formed of marine-derived *Penicillium janthinellum* mycelial pellets for removing dyes from dye-containing wastewater, Chem. Eng. J., 259 (2015) 837–844.

[4] J.A. González, M.E. Villanueva, L.L. Piehl, G.J. Copello, Development of a chitin/graphene oxide hybrid composite for the removal of pollutant dyes: adsorption and desorption study, Chem. Eng. J., 280 (2015) 41–48.

[5] A. Ghosh, A. Mondal, Fabrication of stable, efficient and recyclable p-CuO/n-ZnO thin film heterojunction for visible light driven photocatalytic degradation of organic dyes, Mater. Lett., 164 (2016) 221–224.

[6] R. Liang, F. Jing, L. Shen, N. Qin, L. Wu, MIL-53(Fe) as a highly efficient bifunctional photocatalyst for the simultaneous reduction of Cr(VI) and oxidation of dyes, J. Hazard. Mater., 287 (2015) 364–372.

[7] H.R. Rajabi, M. Farsi, Quantum dot based photocatalytic decolorization as an efficient and green strategy for the removal of anionic dye, Mater. Sci. Semicond. Process., 31 (2015) 478–486.

[8] A.Z. Bouyakoub, B.S. Lartiges, R. Ouhib, S. Kacha, A.G. El Samrani, J. Ghanbaja, O. Barres, $MnCl_2$ and $MgCl_2$ for the removal of reactive dye Levafix Brilliant Blue EBRA from synthetic textile wastewaters: an adsorption/aggregation mechanism, J. Hazard. Mater., 187 (2011) 264–273.

[9] G. Ramírez, F.J. Recio, P. Herrasti, C. Ponce-de-León, I. Sirés, Effect of RVC porosity on the performance of PbO_2 composite coatings with titanate nanotubes for the electrochemical oxidation of azo dyes, Electrochim. Acta, 204 (2016) 9–17.

[10] M.B. Ferreira, J.H.B. Rocha, J.V. de Melo, C.A. Martinez-Huitle, M.A.Q. Alfaro, Use of a dual arrangement of flow cells for electrochemical decontamination of aqueous solutions containing synthetic dyes, Electrocatalysis, 4 (2013) 274–282.

[11] F.D. Castro, J.P. Bassin, M. Dezotti, Treatment of a simulated textile wastewater containing the Reactive Orange 16 azo dye by a combination of ozonation and moving-bed biofilm reactor: evaluating the performance, toxicity, and oxidation by-products, Environ. Sci. Pollut. Res. Int., 24 (2016) 6307–6316.

[12] A. Manivel, G.J. Lee, C.Y. Chen, J.H. Chen, S.H. Ma, T.L. Horng, J.J. Wu, Synthesis of MoO_3 nanoparticles for azo dye degradation by catalytic ozonation, Mater. Res. Bull., 62 (2015) 184–191.

[13] Z.M. Cui, Z. Chen, C.Y. Cao, L. Jiang, W.G. Song, A yolk-shell structured Fe_2O_3@mesoporous SiO_2 nanoreactor for enhanced activity as a Fenton catalyst in total oxidation of dyes, Chem. Commun., 49 (2013) 2332–2334.

[14] L. Hua, H. Ma, L. Zhang, Degradation process analysis of the azo dyes by catalytic wet air oxidation with catalyst CuO/gamma-Al_2O_3, Chemosphere, 90 (2013) 143–149.

[15] Y. Zheng, G. Yao, Q. Cheng, S. Yu, M. Liu, C. Gao, Positively charged thin-film composite hollow fiber nanofiltration membrane for the removal of cationic dyes through submerged filtration, Desalination, 328 (2013) 42–50.

[16] C. Xu, A. Cui, Y. Xu, X. Fu, Graphene oxide–TiO_2 composite filtration membranes and their potential application for water purification, Carbon, 62 (2013) 465–471.

[17] M.E. Fernandez, G.V. Nunell, P.R. Bonelli, A.L. Cukierman, Activated carbon developed from orange peels: batch and dynamic competitive adsorption of basic dyes, Ind. Crops Prod., 62 (2014) 437–445.

[18] X. Peng, D. Huang, T. Odoom-Wubah, D. Fu, J. Huang, Q. Qin, Adsorption of anionic and cationic dyes on ferromagnetic ordered mesoporous carbon from aqueous solution: equilibrium, thermodynamic and kinetics, J. Colloid Interface Sci., 430 (2014) 272–282.

[19] Q. Sun, L. Yang, The adsorption of basic dyes from aqueous solution on modified peat–resin particle, Water Res., 37 (2003) 1535–1544.

[20] Y. Li, Q. Du, T. Liu, X. Peng, J. Wang, J. Sun, Y. Wang, S. Wu, Z. Wang, Y. Xia, L. Xia, Comparative study of methylene blue dye adsorption onto activated carbon, graphene oxide, and carbon nanotubes, Chem. Eng. Res. Des., 91 (2013) 361–368.

[21] T. Madrakian, A. Afkhami, M. Ahmadi, H. Bagheri, Removal of some cationic dyes from aqueous solutions using magnetic-modified multi-walled carbon nanotubes, J. Hazard. Mater., 196 (2011) 109–114.

[22] H. Zhu, Y. Fu, R. Jiang, J. Yao, L. Liu, Y. Chen, L. Xiao, G. Zeng, Preparation, characterization and adsorption properties of chitosan modified magnetic graphitized multi-walled carbon nanotubes for highly effective removal of a carcinogenic dye from aqueous solution, Appl. Surf. Sci., 285 (2013) 865–873.

[23] A. Demirbas, Agricultural based activated carbons for the removal of dyes from aqueous solutions: a review, J. Hazard. Mater., 167 (2009) 1–9.

[24] A. Mittal, J. Mittal, A. Malviya, D. Kaur, V.K. Gupta, Adsorption of hazardous dye crystal violet from wastewater by waste materials, J. Colloid Interface Sci., 343 (2010) 463–473.
[25] E. Haque, J.W. Jun, S.H. Jhung, Adsorptive removal of methyl orange and methylene blue from aqueous solution with a metal-organic framework material, iron terephthalate (MOF-235), J. Hazard. Mater., 185 (2011) 507–511.
[26] G. Jing, L. Wang, H. Yu, W.A. Amer, L. Zhang, Recent progress on study of hybrid hydrogels for water treatment, Colloids Surf., A, 416 (2013) 86–94.
[27] G. Crini, Studies on adsorption of dyes on beta-cyclodextrin polymer, Bioresour. Technol., 90 (2003) 193–198.
[28] I. Popescu, D.M. Suflet, Poly(N-vinyl caprolactam-co-maleic acid) microparticles for cationic dye removal, Polym. Bull., 73 (2015) 1283–1301.
[29] V. Janaki, B.-T. Oh, K. Shanthi, K.-J. Lee, A.K. Ramasamy, S. Kamala-Kannan, Polyaniline/chitosan composite: an eco-friendly polymer for enhanced removal of dyes from aqueous solution, Synth. Met., 162 (2012) 974–980.
[30] V.K. Gupta, R. Kumar, A. Nayak, T.A. Saleh, M.A. Barakat, Adsorptive removal of dyes from aqueous solution onto carbon nanotubes: a review, Adv. Colloid Interface Sci., 193–194 (2013) 24–34.
[31] D. Tasis, N. Tagmatarchis, A. Bianco, M. Prato, Chemistry of carbon nanotubes, Chem. Rev., 106 (2006) 1105–1136.
[32] Q. Li, F. Zhou, J. Yu, X. Jiang, Removal of Pb^{2+} and Cd^{2+} from aqueous solution using thiol-functionalized multi-walled carbon nanotubes as adsorbents, Desal. Wat. Treat., 63 (2017) 158–166.
[33] N. Che, J. Teng, F. Jiao, X. Jiang, X. Hao, J. Yu, Preparation of triethanolamine functionalized carbon nanotube for aqueous removal of Pb(II), Desal. Wat. Treat., 71 (2017) 191–200.
[34] Y. Zhao, H. Chen, J. Li, C. Chen, Hierarchical MWCNTs/Fe_3O_4/PANI magnetic composite as adsorbent for methyl orange removal, J. Colloid Interface Sci., 450 (2015) 189–195.
[35] R. Wang, B. Yu, X. Jiang, J. Yin, Understanding the host-guest interaction between responsive core-crosslinked hybrid nanoparticles of hyperbranched poly(ether amine) and dyes: the selective adsorption and smart separation of dyes in water, Adv. Funct. Mater., 22 (2012) 2606–2616.
[36] M.B. Gholivand, Y. Yamini, M. Dayeni, S. Seidi, E. Tahmasebi, Adsorptive removal of alizarin red-S and alizarin yellow GG from aqueous solutions using polypyrrole-coated magnetic nanoparticles, J. Environ. Chem. Eng., 3 (2015) 529–540.
[37] R. Liu, Y. Guo, G. Odusote, F. Qu, R.D. Priestley, Core-shell Fe_3O_4 polydopamine nanoparticles serve multipurpose as drug carrier, catalyst support and carbon adsorbent, ACS Appl. Mater. Interfaces, 5 (2013) 9167–9171.
[38] D.R. Dreyer, D.J. Miller, B.D. Freeman, D.R. Paul, C.W. Bielawski, Perspectives on poly(dopamine), Chem. Sci., 4 (2013) 3796.
[39] M.E. Lynge, R. van der Westen, A. Postma, B. Stadler, Polydopamine – a nature-inspired polymer coating for biomedical science, Nanoscale, 3 (2011) 4916–4928.
[40] Y. He, J. Wang, H. Zhang, T. Zhang, B. Zhang, S. Cao, J. Liu, Polydopamine-modified graphene oxide nanocomposite membrane for proton exchange membrane fuel cell under anhydrous conditions, J. Mater. Chem. A, 2 (2014) 9548.
[41] X. Jia, M. Xu, Y. Wang, D. Ran, S. Yang, M. Zhang, Polydopamine-based molecular imprinting on silica-modified magnetic nanoparticles for recognition and separation of bovine hemoglobin, Analyst, 138 (2013) 651–658.
[42] S.K. Li, Y.X. Yan, J.L. Wang, S.H. Yu, Bio-inspired in situ growth of monolayer silver nanoparticles on graphene oxide paper as multifunctional substrate, Nanoscale, 5 (2013) 12616–12623.
[43] Q. Liu, N. Wang, J. Caro, A. Huang, Bio-inspired polydopamine: a versatile and powerful platform for covalent synthesis of molecular sieve membranes, J. Am. Chem. Soc., 135 (2013) 17679–17682.
[44] X.H. Zhao, F.P. Jiao, J.G. Yu, Y. Xi, X.Y. Jiang, X.Q. Chen, Removal of Cu(II) from aqueous solutions by tartaric acid modified multi-walled carbon nanotubes, Colloids Surf., A, 476 (2015) 35–41.
[45] M. Doğan, Y. Özdemir, M. Alkan, Adsorption kinetics and mechanism of cationic methyl violet and methylene blue dyes onto sepiolite, Dyes Pigm., 75 (2007) 701–713.
[46] S.J. Allen, G. McKay, J.F. Porter, Adsorption isotherm models for basic dye adsorption by peat in single and binary component systems, J. Colloid Interface Sci., 280 (2004) 322–333.
[47] S. Chowdhury, R. Mishra, P. Saha, P. Kushwaha, Adsorption thermodynamics, kinetics and isosteric heat of adsorption of malachite green onto chemically modified rice husk, Desalination, 265 (2011) 159–168.